

Hierarchical nesting of slow oscillations, spindles and ripples in the human hippocampus during sleep

Bernhard P Staresina^{1,2,10}, Til Ole Bergmann^{3–6,10}, Mathilde Bonnefond³, Roemer van der Meij³, Ole Jensen³, Lorena Deuker³, Christian E Elger⁷, Nikolai Axmacher^{7–9} & Juergen Fell⁷

During systems-level consolidation, mnemonic representations initially reliant on the hippocampus are thought to migrate to neocortical sites for more permanent storage, with an eminent role of sleep for facilitating this information transfer. Mechanistically, consolidation processes have been hypothesized to rely on systematic interactions between the three cardinal neuronal oscillations characterizing non-rapid eye movement (NREM) sleep. Under global control of de- and hyperpolarizing slow oscillations (SOs), sleep spindles may cluster hippocampal ripples for a precisely timed transfer of local information to the neocortex. We used direct intracranial electroencephalogram recordings from human epilepsy patients during natural sleep to test the assumption that SOs, spindles and ripples are functionally coupled in the hippocampus. Employing cross-frequency phase-amplitude coupling analyses, we found that spindles were modulated by the up-state of SOs. Notably, spindles were found to in turn cluster ripples in their troughs, providing fine-tuned temporal frames for the hypothesized transfer of hippocampal memory traces.

How are new experiences transformed into lasting memory traces? According to two-stage models of memory formation, mnemonic representations are initially reliant on the hippocampus, one of the key regions of the medial temporal lobe (MTL) memory system. During the ‘consolidation’ process, these representations are thought to migrate to neocortical sites for more permanent storage^{1–3}. There is consensus that non-rapid eye movement (NREM) sleep facilitates consolidation (particularly for declarative, that is, hippocampus-dependent, mnemonic contents) in the absence of interference by conscious information processing⁴. Yet, the precise neuronal mechanisms underlying this hippocampal-neocortical dialog remain unknown.

Neuronal information transfer requires a precise temporal structure, which, during sleep (in the absence of external stimuli), has to be provided by spontaneous brain activity itself. NREM sleep is hallmarked by three cardinal neuronal oscillations that may provide the temporal scaffold for such information transfer^{2,5}. First, SOs (~0.75 Hz) reflect global fluctuations in cellular excitability resulting from alternating phases of joint hyperpolarization (down-states) and depolarization (up-states) of large neuron populations^{6,7}. SOs emerge spontaneously in neocortical (mainly prefrontal) regions, even after cortical de-afferentation⁸. Despite the existence of local SOs⁹, they typically reflect traveling waves encompassing the entire neocortex¹⁰, the hippocampus⁹ and the thalamus, where they trigger the release of sleep spindles^{11,12}. Note that 1–4-Hz ‘slow waves’ are sometimes combined with SOs to denote slow wave activity (SWA), but we

primarily focused on the ~0.75 Hz SO^{4,6}. Second, spindles, ~12–16-Hz oscillations of waxing and waning amplitude, are generated among reticular thalamic and thalamo-cortical neurons, the latter of which also project them back into neocortex¹² and the hippocampus^{13,14}. Thus, corticothalamic SO input not only causes the temporal grouping of spindles into SO up-states^{12,15}, but also their spatial synchronization throughout the neocortex, notwithstanding the existence of local spindles¹³. Finally, ripples are high-frequency bursts, observed at ~200 Hz in the CA1 subregion of the rodent hippocampus¹⁶, but at lower frequencies of ~80–100 Hz in human hippocampal recordings^{17–20}, that accompany reactivation of local memory traces²¹.

According to the influential ‘active consolidation’ framework put forth previously, information transfer in the service of memory consolidation relies on the intricate interplay of these three electrophysiological phenomena^{4,5}: the depolarizing SO up-states are thought to facilitate the emergence of spindles, which in turn bundle local information units (ripples) in the hippocampus and shuttle them to distributed neocortical sites for long-term storage. Notably, this model implies that, in the hippocampus, the up-states of SOs arriving from the neocortex coincide with spindles arriving from the thalamus to group ripples and thereby initiate the hippocampal-neocortical dialog. Using direct intracranial recordings, we found evidence supporting the hierarchical nesting of these three key oscillations in the human hippocampus, thereby offering a mechanistic account for neuronal information transfer during human NREM sleep.

¹School of Psychology, University of Birmingham, Birmingham, UK. ²MRC Cognition and Brain Sciences Unit, Cambridge, UK. ³Donders Institute for Brain, Cognition and Behaviour, Radboud University Nijmegen, Nijmegen, the Netherlands. ⁴Institute of Psychology, Christian-Albrechts-University of Kiel, Kiel, Germany. ⁵Department of Neurology and Stroke, and Hertie Institute for Clinical Brain Research, University of Tübingen, Tübingen, Germany. ⁶Institute for Medical Psychology and Behavioral Neurobiology, University of Tübingen, Tübingen, Germany. ⁷Department of Epileptology, University of Bonn, Bonn, Germany. ⁸German Center for Neurodegenerative Diseases (DZNE), Bonn, Germany. ⁹Department of Neuropsychology, Institute of Cognitive Neuroscience, Ruhr University Bochum, Bochum, Germany. ¹⁰These authors contributed equally to this work. Correspondence should be addressed to B.P.S. (b.staresina@bham.ac.uk).

Received 23 June; accepted 18 August; published online 21 September 2015; doi:10.1038/nn.4119



RESULTS

We analyzed intracranial electroencephalogram (iEEG) recordings from 12 patients with pharmaco-resistant epilepsy. Hippocampal depth electrodes were implanted bilaterally, and only electrodes from the non-pathological hemisphere according to clinical monitoring were analyzed (except for one patient with unilateral implantations and a neocortical lesion and focus). **Figure 1a** shows the post-operative magnetic resonance image (MRI, with depth electrodes) along with the co-registered pre-operative MRI (without depth electrodes) for a sample participant (electrode locations for all participants are shown in **Supplementary Fig. 1**). Across participants, nightly recordings lasted, on average, 10.65 h (s.d. = 2.92 h), of which an average of 8.42 h (s.d. = 2.00 h) were spent in sleep stages 1–4 or REM sleep²². **Figure 1b** shows a sample hypnogram of one participant. Proportions of times spent in each stage are listed in **Supplementary Table 1**. The NREM sleep epochs that we analyzed included stages 2, 3 and 4 (ref. 22).

To assess the functional coupling of SOs, spindles and ripples, we pursued two complementary analytical approaches, both of which queried whether the amplitude (power) of a faster oscillation is systematically modulated by the phase of a slower oscillation (phase-amplitude coupling, PAC). First, using an event-locked analysis, we specifically tested the hypothesized nesting of SOs, spindles and ripples based on these phenomena's a priori defined frequency ranges. We selectively identified SO, spindle and ripple events in the hippocampal iEEG according to established detection algorithms^{15,23} and aligned time-frequency representations (TFRs) of the peri-event epochs to the center of the respective events of interest (Online Methods). SO-to-spindle PAC (0.75 Hz to 12–16 Hz) and spindle-to-ripple PAC (12–16 Hz to 80–100 Hz) would therefore emerge as power modulation over time in the respective event-locked TFR. Second, using a comodulogram analysis²⁴, we simultaneously assessed PAC across a wider range of frequency pairs to test the selectivity of SO-spindle-ripple coupling and to explore whether there are other cross-frequency interactions that have not yet been incorporated into models of hippocampal processing during sleep.

Event-locked analysis

Our automated event detection algorithm yielded an average of 545 SOs (s.d. = 236), 821 spindles (s.d. = 470) and 166 ripples (s.d. = 88) in the hippocampus per participant. **Supplementary Table 2** also lists the event densities (number of occurrences per minute) for each participant, which were on average 3.7 (s.d. = 0.8) for SOs, 5.4 (s.d. = 2.2) for spindles and 1.2 (s.d. = 0.7) for ripples. Notably, we explored a wide range of detection criteria (yielding different numbers of events) and found that results were markedly robust irrespective of the particular thresholds applied (**Supplementary Table 3**).

SOs and spindles detected with scalp electrodes (Cz). Before detecting events in the hippocampus, we wanted to ensure that our implementation of the SO and spindle detection algorithms would replicate results found at scalp electrode Cz. Indeed, **Supplementary Figure 2**, depicting the TFR time-locked to the SO down-state (trough), shows the typical modulation of spindle power (12–16 Hz) during the SO event. Specifically, spindle power was decreased during the SO down-state, increased during the subsequent down-to-up transition, peaked during the SO up-state and showed a lasting suppression following the SO event^{15,23}. The preferred phases of this SO-spindle modulation clustered significantly around the up-state across participants ($V = 6.55$, $P = 0.004$, average preferred phase = 328°; for PAC analysis details, see Online Methods). Conversely, power in

the 8–12-Hz range (including slow spindle power) showed the opposite pattern with increases during the SO up-to-down transition²³.

Hippocampal SOs group spindles. SO-spindle interactions have been well established in scalp EEG¹⁵ (see above) as well as in invasive cortical and thalamic recordings in the cat¹², but whether they also exist in the human hippocampus is unknown. The unfiltered hippocampal iEEG trace, time-locked to the down-state of detected hippocampal SO events, is shown in **Figure 2a** (note that SO up-states correspond to peaks and down-states to troughs of the scalp EEG, whereas the opposite is true for iEEG depth recordings⁹). **Figure 2b** depicts the corresponding grand average hippocampal TFR, expressed in power change relative to a pre-SO interval of –2.5 s to –1.5 s. Notably, spindle power (12–16 Hz) showed a significant increase in the SO up-state, that is, averaged from +250 ms to +750 ms relative to the maximal SO down-state (45.6% increase, s.d. = 40.5, $t(11) = 3.90$, $P = 0.003$). **Figure 2c** shows a significant spindle cluster emerging in the SO up-state after statistical thresholding ($P < 0.05$, corrected). Across participants, the maximum power increase occurred at 14.5 Hz (s.d. = 2.8, within a search interval of 10–20 Hz, averaged from +250 ms to +750 ms relative to the maximal SO down-state). Indeed, the preferred phases of this SO-spindle modulation clustered significantly toward the SO up-state across participants ($V = 7.78$, $P = 0.0007$, average preferred phase = 160°). **Figure 2d** shows data from a single participant to better illustrate the modulation of the spindle power by the SO up-state. Note also that **Figure 2b** hints to an increase of ripple power concurrent with the spindle power increase, which we examine further below.

Although SOs in Cz showed the known grouping of both fast (12–16 Hz) and slow (8–12 Hz) spindles in their up- and down-states, respectively²³, SOs in the hippocampus (HC) only grouped fast spindles. To quantify these cross-regional differences in SO-spindle_{slow} modulations, we defined the slow spindle range from 8–12 Hz²³ and the fast spindle range (as previously) from 12–16 Hz. The time window for the SO down-state was set from –250 ms to +250 ms around the Cz trough or HC peak, and for the SO up-state from +250 ms to +750 ms relative to the Cz trough or HC peak. Although the increase in fast spindle power during the SO up-state was significant in both Cz and HC (both $t(11) > 3.89$, $P < 0.004$, see also **Supplementary Table 3**), the increase in slow spindle power during the SO down-state was only significant in Cz ($t(11) = 4.76$, $P = 0.001$) but not in HC ($t(11) = 1.71$, $P = 0.115$). A significant region (Cz, HC) × spindle (slow, fast)

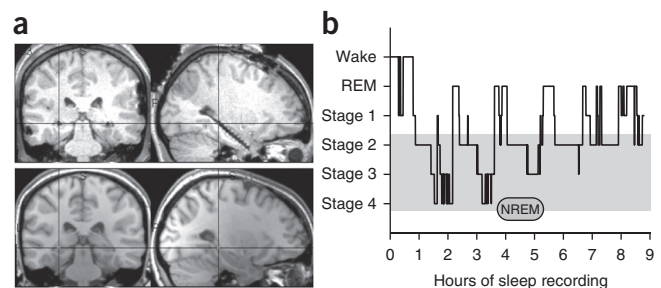


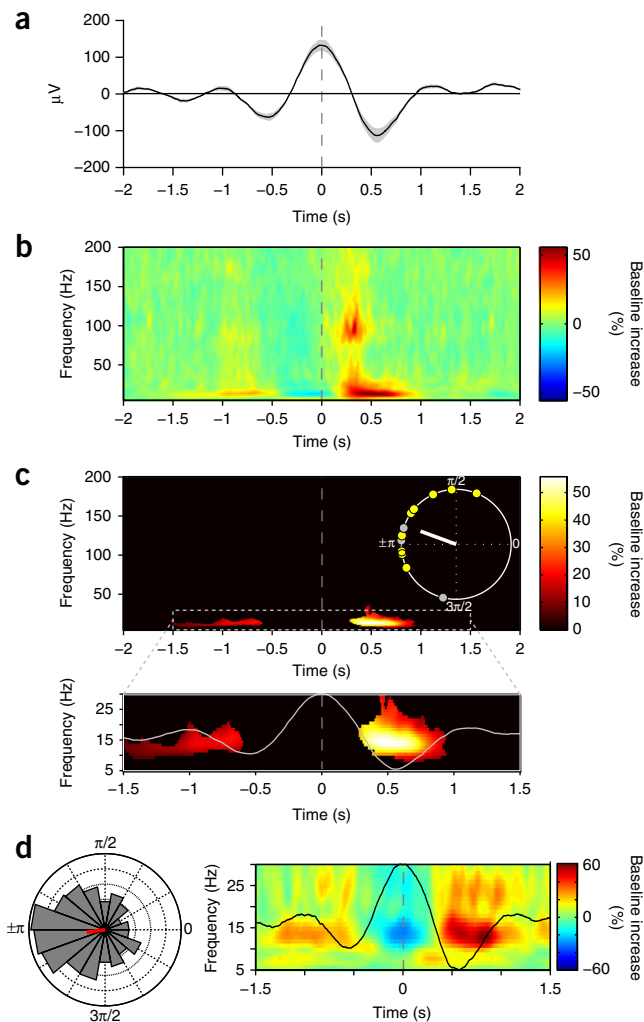
Figure 1 Implantation and sleep recordings. **(a)** Post-operative MRI (top) and co-registered pre-operative MRI (bottom) for a sample participant showing a depth electrode implanted along the longitudinal axis of the hippocampus (**Supplementary Fig. 1** shows electrode locations for all participants). Cross-hair is placed on the electrode taken forward to the group analysis (Online Methods). **(b)** Graphic depiction of time spent in different sleep stages across one recording night (hypnogram) for a sample participant.

Figure 2 Event-locked analysis of hippocampal SO-spindle PAC. **(a)** Grand average unfiltered iEEG trace across participants (mean \pm s.e.m.), aligned to the maximum of the SO down-state (peak, time 0). **(b)** Average of SO down-state-locked TFR (percentage change from pre-event baseline). y-axis starts at 5 Hz to circumvent the dominance of power in the SO range. **(c)** Statistically significant change from pre-event baseline ($P < 0.05$, corrected). Inset, unit circle of preferred phases of the SO-spindle modulation for each participant, which illustrates the preferred clustering of spindle power toward the SO up-state (160° , white line). Yellow circles represent participants whose Rayleigh test for non-uniformity was significant at $P < 0.05$. **(d)** Data from a sample participant. Right, average SO and TFR, zoomed in on -1.5 s to $+1.5$ s and on 5–30 Hz to highlight the nesting of spindle power in the SO up-state. Left, normalized histogram (18 bins, 20° each) of preferred SO-spindle modulation phases across all detected SO events ($N = 1015$), resulting in an average preferred phase of 187° for this participant (red line).

interaction ($F(1,11) = 19.67$, $P = 0.001$) also reflected the fact that there was a significant difference between Cz and HC in slow spindle power during the SO down-state ($t(11) = 3.11$, $P = 0.010$), but no difference in fast spindle power during the SO up-state ($t(11) = 1.67$, $P = 0.124$). This finding is consistent with previous studies linking fast rather than slow spindles to hippocampal activity^{25–27} and suggesting different roles of these two spindle types in sleep-dependent memory consolidation^{5,23,28}.

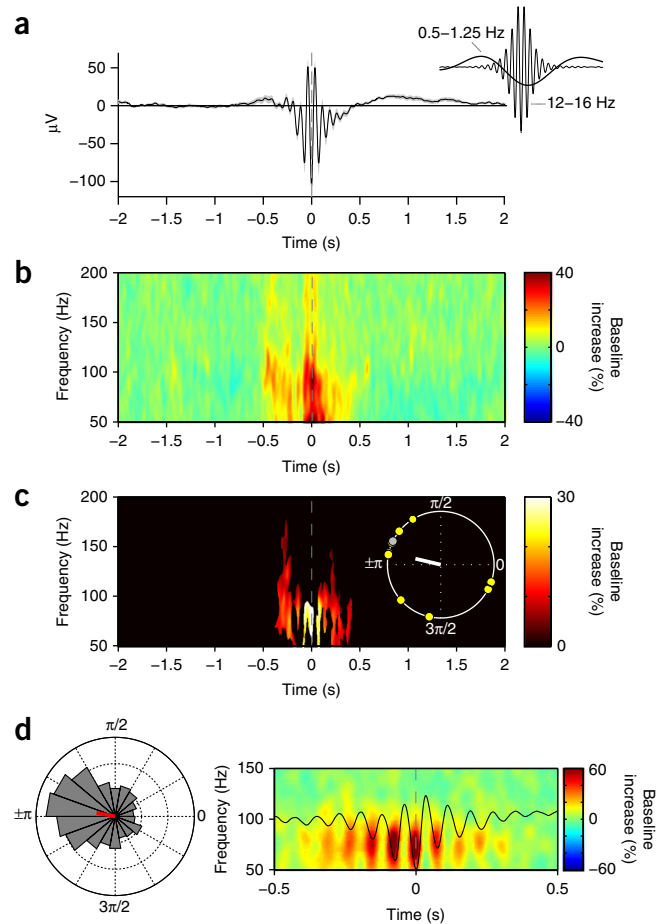
On a separate note, the detected SOs could be either concatenated events (that is, real multi-event oscillations) or solitary events (such as isolated ‘K complexes’). We found that 24.3% (s.d. = 5.2) of all detected hippocampal SOs and 33.5% (s.d. = 7.7) of all detected Cz SOs were preceded or followed by another SO down-state within ± 1.3 s (~ 0.75 Hz), thus being part of a true multi-event oscillation (Supplementary Figs. 3 and 4). All of the measures of PAC were significant for this sub-selection of SOs both in HC and Cz (Supplementary Table 3a). Note that a certain proportion of the remaining ‘solitary’ SOs may still have been preceded or followed by sub-threshold (undetected) small SOs and do not necessarily represent isolated SOs or K complexes (the distinction of which is under debate, with the neurophysiological evidence rather supporting their similarities²⁹).

Hippocampal ripples are nested in spindle troughs. The second key component of two-stage consolidation models is the notion that hippocampal ripples are nested in spindle troughs, thus using fine-grained temporal windows of synaptic excitability to facilitate cross-regional interactions^{1,4,5}. Time-locked to the maximal spindle trough (Fig. 3a), Figure 3b depicts the grand average hippocampal TFR relative to a pre-spindle interval of -2.5 s to -1.5 s. Ripple power (80–100 Hz) showed a significant increase in the 500 ms around the spindle center (17.9% increase, s.d. = 13.5, $t(11) = 4.59$, $P = 0.001$), with a maximum power increase across participants at 86.8 Hz (s.d. = 12.2, within a search interval of 70–110 Hz, averaged from -250 ms to $+250$ ms relative to the spindle center). Notably, discrete ripple power bursts were nested in individual spindle troughs ($P < 0.05$, corrected; Fig. 3c). The preferred phases of this spindle-ripple modulation clustered significantly around the trough across participants ($V = 5.71$, $P = 0.009$, average preferred phase = 167°). Figure 3d shows data from a single participant, highlighting the high temporal precision of ripple nesting in individual spindle cycles. We note that spurious PAC can emerge from non-sinusoidal signals^{30,31}. However, such spurious PAC tends to elicit effects in broadband frequency ranges, unlike the well-circumscribed PAC we observed (Fig. 3) and that precisely matches the frequency range of physiological ripples previously observed in the human hippocampus^{17–20}.



Ripple-locked analysis. Lastly, we examined whether hippocampal spindle-ripple coupling would also emerge when time-locking the hippocampal EEG to discrete ripple occurrences. To this end, we identified ripple events analogous to SOs and spindles (Online Methods). First, ripple-locked EEG confirmed the oscillatory nature of the detected events in the unfiltered raw data (Fig. 4a). Second, it revealed the superimposition of ripples on a pronounced deflection in the delta range, which showed a spectral peak at 3 Hz. The same coupling of ripples with ‘delta waves’ has been observed in both human¹⁷ and non-human primate³² hippocampal recordings. Turning to the ripple-locked TFR (Fig. 4a), we first confirmed, again consistent with previous reports on human ripples^{17,18}, the band-limited nature of the ripples that we identified. Note that the maximum ripple power increase (relative to a pre-event baseline interval of -1.5 s to -1.0 s) occurred at 86.2 Hz across participants (s.d. = 4.0, search interval from 70–110 Hz and from -25 ms to $+25$ ms around the ripple center), which closely matches the frequency in which the spindle-locked power maximum was observed (86.8 Hz). Notably, the peri-event TFR also revealed a significant increase in spindle power (12–16 Hz) in the 500 ms around the ripple center (65.5% increase, s.d. = 50.5, $t(11) = 4.49$, $P = 0.0009$; Fig. 4a). The maximum spindle power increase across participants was observed at 14.6 Hz (s.d. = 3.3, search interval from 10–20 Hz and from -250 ms to $+250$ ms around the ripple center), which corresponds to the frequency of the maximum spindle modulation

Figure 3 Event-locked analysis of hippocampal spindle-ripple PAC. (a) Grand average unfiltered iEEG trace across participants (mean \pm s.e.m.), aligned to the maximum of the spindle trough (time 0). Note that the spindle's mean potential is below zero (-250 ms to $+250$ ms, $t(11) = 3.94$, $P = 0.002$), reflecting the grouping of spindles in the SO trough (as shown in **Fig. 2**). This is further illustrated in the inset, which shows the grand average iEEG trace bandpass filtered from 0.5 – 1.25 Hz (SO range) and from 12 – 16 Hz (spindle range), respectively. (b) Average of spindle-trough-locked TFR (percentage change from pre-event baseline). y axis starts at 50 Hz to circumvent the dominance of power in the spindle range. (c) Statistically significant change from pre-event baseline ($P < 0.05$, corrected). Inset, unit circle of preferred phases of the spindle-ripple modulation for each participant, which illustrates the preferred clustering of ripple power in the spindle trough (167° , white line). Yellow circles represent participants whose Rayleigh test for non-uniformity was significant at $P < 0.05$. (d) Data from one participant. Right, average spindle and TFR, zoomed in on -0.5 s to 0.5 s and on 50 – 150 Hz to illustrate the nesting of ripple power within spindle troughs. Left, normalized histogram (18 bins, 20° each) of preferred spindle-ripple modulation phases across all detected spindle events ($N = 1,487$), resulting in an average preferred phase of 169° for this participant (red line).



by the SO identified above (**Fig. 2**). In **Figure 4b**, we show the average ripple-locked raw EEG trace for the same individual participant described above (**Figs. 2d and 3d**). Note that, when bandpass filtering the EEG trace around that participant's spindle power maximum (14 Hz), the nesting of ripples in the spindle trough again becomes apparent. To further confirm the nesting of ripples in successive spindle troughs, we derived the occurrence probabilities of other ripples relative to a given ripple's center time (ripple-ripple peri-event time histogram, PETH). This ripple-ripple PETH revealed peaks of occurrence probabilities that markedly followed a 14.5 -Hz oscillation (**Fig. 4c**). Finally, although ripple power tended to be maximal just before the spindle maximum, we found that spindle onsets reliably preceded ripple onsets (rather than ripples triggering spindles; **Supplementary Fig. 5**).

Event contingencies. Together, our results provide compelling evidence for the hypothesized modulation of spindles by SOs and for the nesting of hippocampal ripples in the troughs of individual spindle cycles. Lastly, we set out to quantify the contingencies of all three event types, that is, the temporal co-occurrence of SOs, spindles and ripples. First, in the same analytical framework as applied above, we observed significant spindle-ripple coupling when restricting the analysis to spindles that were immediately preceded by SO down-states ($P < 0.05$, corrected; **Supplementary Fig. 6**). Moreover, ripple amplitude (80 – 100 Hz) was significantly modulated by the phase of 12 – 16 -Hz oscillations when calculated from 0.2 – 1 s following the down-state of individual SO events (where spindle power showed a significant increase; **Fig. 2b**) ($V = 5.65$, $P = 0.01$, average preferred phase = 172°). These results provide critical evidence for SO-spindle-ripple coupling in a true hierarchical fashion (see **Supplementary Fig. 7** for example raw traces).

Second, based on our event detection algorithms, 21% of SOs were found to trigger spindles such that the spindle center lies between 0.2 and 1 s after the maximal SO down-state. Of those spindles, 6% also contain ripples within ± 0.5 s around the spindle center. Note however that the outcomes of these analyses greatly depend on both the event detection criteria of SOs, spindles and ripples and the time intervals used to define temporal co-occurrences. For instance, when setting the ripple detection threshold to the top 2% amplitude instead of the top 1% amplitude (**Supplementary Table 3c**), the proportion of

SO-triggered spindles that also contain ripples increases from 6 to 10% . In an additional analysis, we identified which proportion of all ripples (threshold of top 1%) detected during SWS were accompanied by both spindles and SOs (search window of ± 2 s), revealing a proportion of 24% ripples occurring in conjunction with spindles and SOs. Given the dependency of these results on the particular threshold settings, we needed to ensure that the numbers that we obtained indeed reflect co-occurrences of the three event types beyond chance. To this end, we devised a surrogate analysis in which we considered each participant's numbers of detected SOs, spindles and ripples and the number of available data samples after artifact rejection and restriction to NREM sleep. Under the null hypothesis of no systematic interaction between SOs, spindles and ripples, these events would be randomly distributed across the available samples. Deriving $1,000$ of such surrogate distributions, the grand average percentage of spindles that were preceded by an SO (-1 to -0.2 s) and that also contained a ripple within ± 0.5 s around the spindle center was 2% , and no single surrogate iteration reached the empirical value of 6% , such that the observed percentage of SO-spindle-ripple clustering significantly exceeded chance ($P < 0.001$). Likewise, for the proportion of ripples occurring in conjunction with both spindles and SO down-states (± 2 s) during SWS, the grand average surrogate value was 8% , again with no single surrogate iteration reaching the empirical value of 24% ($P < 0.001$).

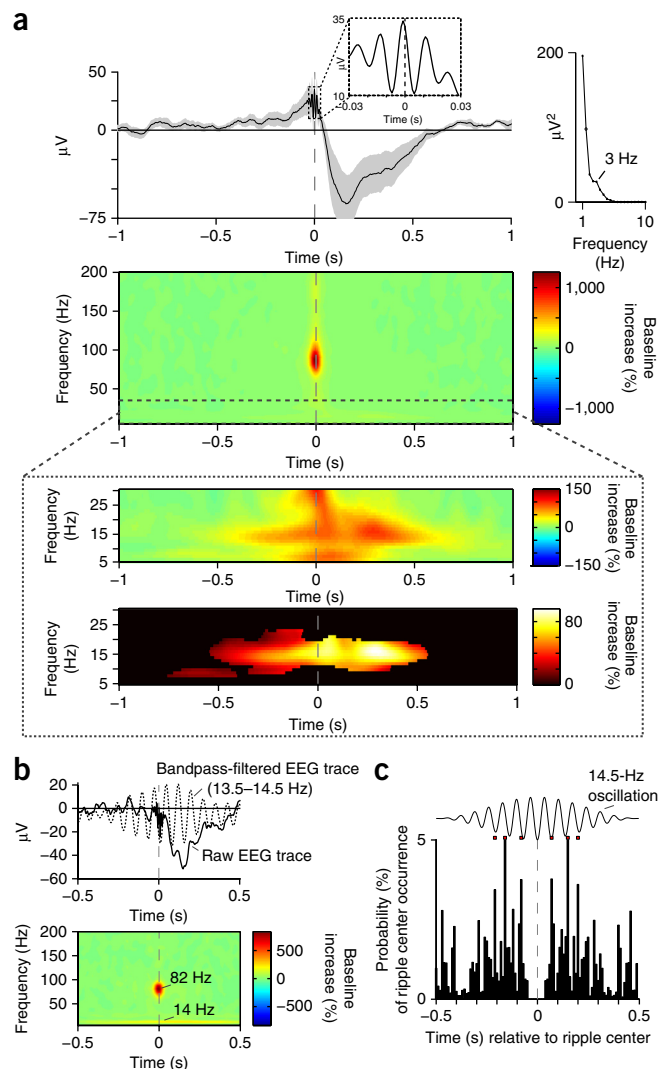
That said, significant spindle-ripple coupling was also observed for the spindles that were not immediately preceded by SO down-states ($P < 0.05$, corrected; **Supplementary Fig. 6**), and it will be important for future studies to examine whether these two types of spindle-ripple coupling differ in their contributions to consolidation processes.

Figure 4 Hippocampal ripples. (a) Top, grand average unfiltered iEEG trace across participants (mean \pm s.e.m.), aligned to the maximum of the ripple peak (time 0). The first inset highlights the oscillatory nature of the detected events in the unfiltered raw EEG. The second inset shows the result from a spectral analysis of the grand average EEG (calculated from -1 s to $+1$ s via FieldTrip's `mtmfft` function for frequencies from 1–10 Hz in steps of 0.5 Hz), revealing a spectral peak at 3 Hz (delta wave). Middle, average of ripple-peak-locked TFR (percentage change from pre-event baseline), highlighting the band-limited nature of ripples. Bottom, zoom into 5–30 Hz, showing the grand-average TFR before (top) and after (bottom) statistical thresholding ($P < 0.05$, corrected) to highlight the ripple-locked increase in spindle power. (b) Data from a sample participant. Top, ripple-locked average raw EEG trace (solid line) with the bandpass-filtered trace (13.5–14.5 Hz, dotted line) superimposed to highlight the nesting of ripples in spindle troughs. Bottom, corresponding ripple-locked TFR, highlighting that participant's maxima in the ripple- and spindle ranges. (c) Ripple-ripple PETH. Occurrence probabilities of other ripples relative to individual ripples' center time. A synthetic 14.5-Hz oscillation is superimposed to illustrate the periodicity of ripple occurrences following successive spindle cycles. Red squares project the histogram maxima from -250 ms to $+250$ ms relative to the ripple center to better visualize the correspondence of occurrences with individual spindle cycles.

Cross-regional PAC. To test whether SOs, spindles and ripples may indeed serve to facilitate hippocampal-neocortical information transfer during sleep, we quantified the coupling of hippocampal spindles and ripples with cortical SOs and spindles, respectively. To this end, we used the scalp electrode Cz (in lieu of intracranial electrodes in other neocortical sites), where the above analysis revealed clearly detectable SOs and spindles (Supplementary Fig. 2). Data segments that were artifact-free in both sites were searched for Cz SOs and spindles as described above and TFRs in the hippocampus were aligned to the respective event centers in Cz. Indeed, we found evidence for both coupling of Cz SOs (SO_{Cz}) to hippocampal spindles ($spindle_{HC}$) and coupling of Cz spindles ($spindle_{Cz}$) to hippocampal ripples ($ripple_{HC}$). For SO_{Cz} - $spindle_{HC}$ coupling, there was a 20.5% (s.d. = 29.5) increase in hippocampal spindle power during the up-state of the Cz SO (250–750 ms, $t(11) = 2.41$, $P = 0.035$). Likewise, for $spindle_{Cz}$ - $ripple_{HC}$ coupling, there was a 4.8% (s.d. = 4.9) increase in hippocampal ripple power from -250 ms to $+250$ ms around the Cz spindle center ($t(11) = 3.41$, $P = 0.006$).

We reasoned that, mechanistically, such cross-regional PAC would most likely be implemented by the synchronizing effect of SOs and spindles that temporally co-occur across neocortex and the hippocampus. Deriving the co-occurrence probabilities of SOs and spindles across Cz and HC (Supplementary Fig. 8), we found that 19.1% (s.d. = 3.3) of SO_{Cz} were accompanied by SO_{HC} within ± 0.5 s and 33.5% (s.d. = 8.5) of $spindle_{Cz}$ were accompanied by $spindle_{HC}$ within ± 0.5 s. Note that the numbers of detected SOs and spindles necessarily depend on the specific detection criteria, but the proportions of SOs and spindles co-occurring across Cz and HC are consistent with the proportions of slow waves and spindles that were previously reported⁹ to occur 'globally' (in more than 50% of recorded intracranial sites; 15% slow waves and 34% spindles).

As anticipated, SO_{Cz} - $spindle_{HC}$ coupling was significantly greater (and significantly different from 0 only) for the 19.1% SO_{Cz} that co-occurred with SO_{HC} compared with those SO_{Cz} that did not co-occur with SO_{HC} (55.0 versus 12.5% spindle power increase, $t(11) = 2.61$, $P = 0.024$). Likewise, $spindle_{Cz}$ - $ripple_{HC}$ coupling was significantly greater (and significantly different from 0 only) for the 33.5% $spindle_{Cz}$ that co-occurred with $spindle_{HC}$ compared with those $spindle_{Cz}$ that did not co-occur with $spindle_{HC}$ (12.0 versus 0.6% ripple power increase, $t(11) = 4.85$, $P = 0.001$).



However, the distribution of preferred phases for SO_{Cz} - $spindle_{HC}$ coupling and for $spindle_{Cz}$ - $ripple_{HC}$ coupling was not reliable across participants (irrespective of whether all SO_{Cz} and $spindle_{Cz}$ were used or only those co-occurring with SO_{HC} and $spindle_{HC}$ and irrespective of whether an a priori hypothesized mean phase angle was defined (V test) or not (Rayleigh test), all $P > 0.07$). Although this is probably not surprising given that the scalp Cz electrode aggregates neocortical SOs and spindles across numerous neural generators, it emphasizes that establishing a temporally more fine-tuned cross-regional PAC between a particular neocortical region and the hippocampus would greatly benefit from concurrent intracranial recordings in both sites^{9,11,33,34}.

Comodulogram analysis

After directly testing the hypothesized PAC across pre-defined oscillatory events (SOs, spindles and ripples), we set out to explore hippocampal PAC across a more exhaustive frequency range. An effective one-step and data-driven procedure to uncover PAC across a wider frequency range is the PAC comodulogram method introduced previously³⁵. Conceptually, the critical modulation index (MI) is a PAC measure similar to the PAC measure used for the event-locked analysis in that it reflects the extent to which the amplitude of the modulated (higher) frequency varies as a function of the phase of the modulating (lower) frequency (see Online Methods). Hippocampal

Figure 5 Hippocampal PAC during NREM sleep. Clusters showing a significant MI when comparing NREM PAC versus WAKE PAC and NREM PAC versus trial-shuffled NREM surrogate data. Both contrasts were thresholded at $P < 0.05$ (two-tailed paired-sample t tests), and significant clusters were defined as a minimum of 25 contiguous frequency pairs showing significant differences in both contrasts. Effect sizes are scaled in each cluster to a maximum of 1 and a minimum of 0 (separate unscaled comodulograms for each comparison are shown in **Supplementary Fig. 9**). Insets show average amplitudes of the modulated frequency as a function of 1.5 cycles of the modulating frequency's phase, with y axes ranging from minimum to maximum amplitude modulation.

PAC during NREM sleep was identified as the conjunction of two contrasts. First, to reveal PAC specific to NREM sleep, we identified frequency pairs in which the MI was greater for NREM than for WAKE. Second, to ensure that the resulting effects are not biased by greater amplitudes during NREM, we derived trial-shuffled surrogate data in which the same data were used as for the real PAC analysis (that is, showing exactly the same spectral power characteristics) and compared them with the original NREM data.

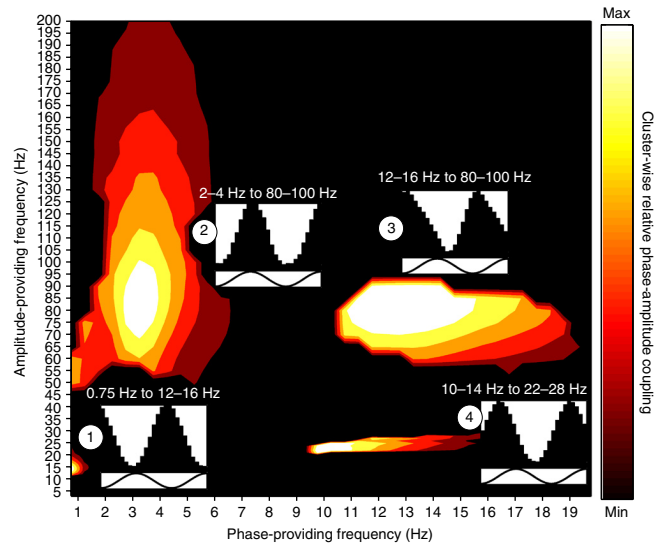
Four clusters resulted from this procedure (**Fig. 5**). Cluster 1 replicates the SO-spindle PAC observed in the event-locked analysis, with the maximum at the phase of a 0.75-Hz oscillation modulating the amplitude of 14-Hz activity. Cluster 2 replicates the modulation of ripple power by oscillations in the delta range, showing its maximum at the phase of a 3.25-Hz oscillation modulating the amplitude of 85 Hz activity. Cluster 3 replicates the spindle-ripple PAC observed in the event-locked analysis, with the maximum at the phase of a 12.75-Hz oscillation modulating the amplitude of 85-Hz activity. Note that across clusters 2 and 3, the preferred phase of the 80–100-Hz amplitude modulation differed reliably (cluster \times phase bin interaction, $F(1.42, 15.66) = 4.43$, $P = 0.041$), indicating that ripples are nested in spindle troughs but occur at the peak of the delta oscillation. Finally, an additional cluster emerged (cluster 4), with the maximum modulation occurring at the phase of a 10.25-Hz oscillation modulating amplitude at 22 Hz (slow spindle-beta PAC).

These results not only corroborate the main findings from our event-based analysis, but they also highlight the relative selectivity of hippocampal PAC to SO-spindle and spindle-ripple interactions. Slow spindle-beta PAC, although not a component of current systems-consolidation accounts, has recently been reported in sleep scalp EEG recordings³⁶.

DISCUSSION

Although the role of NREM sleep for memory consolidation has long been recognized^{4,37}, the precise mechanisms of the hypothesized hippocampal-neocortical dialog have remained elusive. Extant models, first and foremost the active consolidation framework^{4,5}, hold that memory consolidation relies on an intricate interaction of the three cardinal NREM sleep signatures, SOs, spindles and ripples. In particular, under the global influence of neocortical SOs, thalamocortical spindles are thought to group hippocampal ripples in the service of temporally fine-tuned information transfer between the hippocampus and neocortex. We used direct electrophysiological recordings to test the tacit assumption that SOs, spindles and ripples coincide and systematically interact in the human hippocampus.

In compelling agreement with this conjecture, our results suggest that sleep spindles recorded in the hippocampus are orchestrated by SOs and that spindles in turn nest hippocampal ripples in their troughs. This pattern was observed using two complementary analyses. Using an event-locked analysis, we identified SO and spindle events on the basis of established detection algorithms and we used



the event centers to align the TFR of faster neuronal oscillations. This analysis revealed a strong increase in the spindle frequency power (12–16 Hz) around the trough of the hippocampal SO (**Fig. 2**), that is, beginning at the transition of hippocampal down-to up-states⁹, analogous to the SO-spindle modulation typically observed in scalp recordings²³ (**Supplementary Fig. 2**). When in turn aligning the TFR to spindle event centers (**Fig. 3**), the emergence of ripple bursts nested in the spindle troughs became apparent. Finally, the same spindle-ripple coupling emerged when identifying individual ripple events in our data. Not only did the ripple-locked TFR reveal a strong spindle power increase (**Fig. 4a**), but successive ripple occurrences showed a periodicity that precisely followed a spindle oscillation (**Fig. 4c**).

Our second analysis employed a comodulogram procedure to assess, in one step, the phase-amplitude coupling of an exhaustive range of frequency pairs. This analysis strongly corroborated the findings from the event-locked analysis (**Fig. 5**). Note that the same phase-to-amplitude relationship, that is, spindle power increasing toward the SO trough and nesting of ripples in the spindle trough, emerged in both analyses. It deserves mention that, although we ruled out spurious effects from the mastoid reference electrode (**Supplementary Fig. 10**), our macroelectrode recordings remained agnostic about the precise neural generators underlying the recorded signals^{38,39}. For instance, a recent study found that SOs recorded in the human hippocampus propagate from (prefrontal) neocortical generators⁹, consistent with the global regulatory effect these sleep events are thought to exert^{4,5,37}. Indeed, the large amplitudes of hippocampal SOs that we observed indicate a participation of hippocampal networks in SO propagation (rather than simple effects of volume conduction), consistent with previous findings⁹.

Although previous studies in both animals and humans have provided evidence for either SO-spindle coupling, SO-ripple coupling or spindle-ripple coupling in or across different brain regions, we provide, to the best of our knowledge, the first evidence that all three oscillations indeed coincide and systematically interact in the hippocampus, a key prerequisite for their putative role in facilitating hippocampal consolidation processes. For instance, in a number of rodent recordings, hippocampal ripples have been related to neocortical SWA or spindles^{11,34,38,40}, but not to SWA or spindles recorded in the hippocampus itself. A previous study³⁹ did identify SOs in the rodent hippocampus, but did not relate them to spindles or ripples occurring in the hippocampus or elsewhere. A recent study in

non-human primates⁴¹ reported phase-amplitude coupling between SOs and high-frequency activity in the hippocampus. However, for methodological reasons, the high-frequency range was restricted to 30–80 Hz (which does not allow for the investigation of ripple activity) and spindles were not investigated in that study. Finally, another study⁴² reported a modulation of hippocampal high-frequency activity by the phase of hippocampal spindle oscillations in rats. However, these analyses were mainly based on the waking and REM state and not on NREM sleep, and the mediating role of slow waves (or SOs) remained unexamined. In humans, a recent iEEG study⁹ showed that hippocampal ripples preferentially occur during particular phases of hippocampal SWA, but the relationship to spindles was not explored. In a follow-up analysis that focused on spindles¹³, the authors were able to demonstrate that physiological spindles indeed occurred in the human hippocampus (as we observed; **Fig. 3a**), but the relationship of those hippocampal spindles to SOs or ripples was not examined. Another human iEEG study¹⁹ used foramen ovale electrodes to measure ripples in the parahippocampal cortex and related ripple occurrences to cortical SOs and spindles detected with scalp electrodes. Although a consistent temporal relationship was observed across cortical SOs, cortical spindles and parahippocampal ripples, it remains open whether a similar relationship exists among all three oscillations in the human hippocampus (note that foramen ovale electrodes cannot reliably detect physiological activation in the hippocampus⁴³). Finally, a recent EEG-magnetoencephalography (MEG) study conducted in healthy participants found that spindles clustered 40–100-Hz oscillations recorded at the scalp, but the location of the neural generators remained unknown⁴⁴.

Another hippocampal PAC relationship that emerged in both analyses was a prominent modulation of ripple power by oscillations in the delta frequency band (with a maximum at ~3 Hz). Delta range modulation has been observed for ripples recorded in humans during a post-learning nap¹⁷, as well as in recent recordings of ripples in non-human primates³². Whether this phenomenon reflects ripples being modulated by classical delta waves (characteristic of NREM sleep but distinguishable from SOs⁶) or corresponds to sharp-wave-ripple complexes⁴⁵ and whether it is involved in the hypothesized hippocampal-neocortical dialog remain to be determined. On a related note, it deserves mention that the ripple frequency range we report (80–100 Hz) is markedly lower than the range typically observed in rodents (up to ~200 Hz¹⁶). However, 80–100 Hz is precisely where human ripple maxima have been observed^{17–19}, which, alongside recent data showing ripples between 80 and 140 Hz in non-human primates^{32,46}, fits with the notion that functionally homologous oscillations occur at increasingly lower frequencies as brain size increases across species⁴⁷.

Despite the importance of showing the functional coupling of SOs, spindles and ripples within the human hippocampus, our data also support the notion of cross-regional coupling inherent in two-stage models of memory consolidation^{2,4,5}. In particular, we found an increase in hippocampal spindle power time-locked to SOs recorded in Cz as well as an increase in hippocampal ripple power time-locked to spindles recorded in Cz. Moreover, we were able to show that such cross-regional PAC is driven by the temporal co-occurrence of SOs and spindles across Cz and the hippocampus (**Supplementary Fig. 8**), providing further support for the putative hippocampal-neocortical information transfer during sleep.

A pressing question is whether the observed PAC effects directly relate to episodic memory. SO amplitudes have been found to increase during NREM sleep after a hippocampus-dependent learning task⁴⁰, and external facilitation of SOs during NREM sleep boosts subsequent memory

retrieval⁴⁸. Likewise, spindle density was found to increase after learning and to predict later memory performance⁴⁹ and a recent EEG-fMRI study found that spindle power recorded at the scalp strongly correlated with BOLD activation in the hippocampus, with concomitant activation in category-specific brain regions suggesting reactivation of previously learned information²⁷. Notably, this spindle-BOLD correlation was strongest in posterior hippocampus, where we also observed the relative spindle maximum (**Supplementary Fig. 1**). Finally, hippocampal ripples have consistently been related to replay of previous experiences in rodents^{21,46}, their experimental disruption was found to impair spatial memory⁵⁰ and a recent iEEG study in humans revealed that the number of ripples recorded in the human MTL correlated with later memory performance¹⁷. In short, each of these NREM sleep oscillations on their own has been related to memory performance. However, it remains to be determined whether it may ultimately be their systematic interaction that reflects effective reactivation and consolidation during sleep.

To conclude, using the rare opportunity to directly record from the human hippocampus during natural sleep, we found an intricate relationship among the cardinal signatures of NREM sleep. Hippocampal ripples were nested in the troughs of sleep spindles, which in turn were modulated by the phase of SOs. As suggested by extant models of systems-level consolidation, this functional coupling hierarchy may provide a vital mechanism for temporally fine-tuned communication between the hippocampus and neocortex during sleep.

METHODS

Methods and any associated references are available in the [online version of the paper](#).

Note: Any Supplementary Information and Source Data files are available in the [online version of the paper](#).

ACKNOWLEDGMENTS

The research was supported by a Sir Henry Wellcome Fellowship (WT089049AIA) to B.P.S., the BrainGain Smart Mix Programme of the Netherlands Ministry of Economic Affairs (T.O.B.), the VICI grant (453-09-002) from the NWO (O.J.) and the DFG grants AX82/2, AX82/3 (N.A.) and SFB1089 (N.A. and J.F.).

AUTHOR CONTRIBUTIONS

B.P.S. and T.O.B. analyzed the data. B.P.S., T.O.B. and J.F. wrote the manuscript. L.D. acquired data. B.P.S., T.O.B., M.B., R.v.d.M., O.J., N.A. and J.F. provided analytical tools. C.E.E. supervised intracranial recordings.

COMPETING FINANCIAL INTERESTS

The authors declare no competing financial interests.

Reprints and permissions information is available online at <http://www.nature.com/reprints/index.html>.

- Born, J., Rasch, B. & Gais, S. Sleep to remember. *Neuroscientist* **12**, 410–424 (2006).
- Buzsáki, G. The hippocampo-neocortical dialogue. *Cereb. Cortex* **6**, 81–92 (1996).
- McClelland, J.L., McNaughton, B.L. & O'Reilly, R.C. Why there are complementary learning systems in the hippocampus and neocortex: insights from the successes and failures of connectionist models of learning and memory. *Psychol. Rev.* **102**, 419 (1995).
- Rasch, B. & Born, J. About sleep's role in memory. *Physiol. Rev.* **93**, 681–766 (2013).
- Diekelmann, S. & Born, J. The memory function of sleep. *Nat. Rev. Neurosci.* **11**, 114–126 (2010).
- Achermann, P. & Borbely, A. Low-frequency (<1 Hz) oscillations in the human sleep electroencephalogram. *Neuroscience* **81**, 213–222 (1997).
- Steriade, M., Nunez, A. & Amzica, F. A novel slow (<1 Hz) oscillation of neocortical neurons in vivo: depolarizing and hyperpolarizing components. *J. Neurosci.* **13**, 3252–3265 (1993).
- Timofeev, I., Grenier, F., Bazhenov, M., Sejnowski, T. & Steriade, M. Origin of slow cortical oscillations in deafferented cortical slabs. *Cereb. Cortex* **10**, 1185–1199 (2000).
- Nir, Y. *et al.* Regional slow waves and spindles in human sleep. *Neuron* **70**, 153–169 (2011).
- Massimini, M., Huber, R., Ferrarelli, F., Hill, S. & Tononi, G. The sleep slow oscillation as a traveling wave. *J. Neurosci.* **24**, 6862–6870 (2004).

11. Sirota, A., Csicsvari, J., Buhl, D. & Buzsáki, G. Communication between neocortex and hippocampus during sleep in rodents. *Proc. Natl. Acad. Sci. USA* **100**, 2065–2069 (2003).
12. Steriade, M. Grouping of brain rhythms in corticothalamic systems. *Neuroscience* **137**, 1087–1106 (2006).
13. Andrillon, T. *et al.* Sleep spindles in humans: insights from intracranial EEG and unit recordings. *J. Neurosci.* **31**, 17821–17834 (2011).
14. Sarasso, S. *et al.* Hippocampal sleep spindles preceding neocortical sleep onset in humans. *Neuroimage* **86**, 425–432 (2014).
15. Mölle, M., Marshall, L., Gais, S. & Born, J. Grouping of spindle activity during slow oscillations in human non-rapid eye movement sleep. *J. Neurosci.* **22**, 10941–10947 (2002).
16. Buzsáki, G., Horvath, Z., Urioste, R., Hetke, J. & Wise, K. High-frequency network oscillation in the hippocampus. *Science* **256**, 1025–1027 (1992).
17. Axmacher, N., Elger, C.E. & Fell, J. Ripples in the medial temporal lobe are relevant for human memory consolidation. *Brain* **131**, 1806–1817 (2008).
18. Bragin, A., Engel, J., Wilson, C.L., Fried, I. & Buzsáki, G. High-frequency oscillations in human brain. *Hippocampus* **9**, 137–142 (1999).
19. Clemens, Z. *et al.* Temporal coupling of parahippocampal ripples, sleep spindles and slow oscillations in humans. *Brain* **130**, 2868–2878 (2007).
20. Clemens, Z. *et al.* Fine-tuned coupling between human parahippocampal ripples and sleep spindles. *Eur. J. Neurosci.* **33**, 511–520 (2011).
21. Wilson, M.A. & McNaughton, B.L. Reactivation of hippocampal ensemble memories during sleep. *Science* **265**, 676–679 (1994).
22. Rechtschaffen, A. & Kales, A. *A Manual of Standardized Terminology, Techniques and Scoring for Sleep Stages of Human Subjects*. Brain Information Service (Brain Research Institute, University of California, Los Angeles, 1968).
23. Mölle, M., Bergmann, T.O., Marshall, L. & Born, J. Fast and slow spindles during the sleep slow oscillation: disparate coalescence and engagement in memory processing. *Sleep* **34**, 1411 (2011).
24. Tort, A.B., Komorowski, R., Eichenbaum, H. & Kopell, N. Measuring phase-amplitude coupling between neuronal oscillations of different frequencies. *J. Neurophysiol.* **104**, 1195–1210 (2010).
25. Andrade, K.C. *et al.* Sleep spindles and hippocampal functional connectivity in human NREM sleep. *J. Neurosci.* **31**, 10331–10339 (2011).
26. Schabus, M. *et al.* Hemodynamic cerebral correlates of sleep spindles during human non-rapid eye movement sleep. *Proc. Natl. Acad. Sci. USA* **104**, 13164–13169 (2007).
27. Bergmann, T.O., Mölle, M., Diedrichs, J., Born, J. & Siebner, H.R. Sleep spindle-related reactivation of category-specific cortical regions after learning face-scene associations. *Neuroimage* **59**, 2733–2742 (2012).
28. Cox, R., Hofman, W.F., de Boer, M. & Talamini, L.M. Local sleep spindle modulations in relation to specific memory cues. *Neuroimage* **99**, 103–110 (2014).
29. Cash, S.S. *et al.* The human K-complex represents an isolated cortical down-state. *Science* **324**, 1084–1087 (2009).
30. Aru, J. *et al.* Untangling cross-frequency coupling in neuroscience. *Curr. Opin. Neurobiol.* **31**, 51–61 (2015).
31. Kramer, M.A., Tort, A.B. & Kopell, N.J. Sharp edge artifacts and spurious coupling in EEG frequency comodulation measures. *J. Neurosci. Methods* **170**, 352–357 (2008).
32. Logothetis, N.K. *et al.* Hippocampal-cortical interaction during periods of subcortical silence. *Nature* **491**, 547–553 (2012).
33. Mölle, M., Yesenko, O., Marshall, L., Sara, S.J. & Born, J. Hippocampal sharp wave-ripples linked to slow oscillations in rat slow-wave sleep. *J. Neurophysiol.* **96**, 62–70 (2006).
34. Siapas, A.G. & Wilson, M.A. Coordinated interactions between hippocampal ripples and cortical spindles during slow-wave sleep. *Neuron* **21**, 1123–1128 (1998).
35. Tort, A.B.L. *et al.* Dynamic cross-frequency couplings of local field potential oscillations in rat striatum and hippocampus during performance of a T-maze task. *Proc. Natl. Acad. Sci. USA* **105**, 20517 (2008).
36. Cox, R., van Driel, J., de Boer, M. & Talamini, L.M. Slow oscillations during sleep coordinate interregional communication in cortical networks. *J. Neurosci.* **34**, 16890–16901 (2014).
37. Tononi, G. & Cirelli, C. Sleep function and synaptic homeostasis. *Sleep Med. Rev.* **10**, 49–62 (2006).
38. Isomura, Y. *et al.* Integration and segregation of activity in entorhinal-hippocampal subregions by neocortical slow oscillations. *Neuron* **52**, 871–882 (2006).
39. Wolansky, T., Clement, E.A., Peters, S.R., Palczak, M.A. & Dickson, C.T. Hippocampal slow oscillation: a novel EEG state and its coordination with ongoing neocortical activity. *J. Neurosci.* **26**, 6213–6229 (2006).
40. Mölle, M., Eschenko, O., Gais, S., Sara, S.J. & Born, J. The influence of learning on sleep slow oscillations and associated spindles and ripples in humans and rats. *Eur. J. Neurosci.* **29**, 1071–1081 (2009).
41. Takeuchi, S. *et al.* Gamma oscillations and their cross-frequency coupling in the primate hippocampus during sleep. *Sleep* **38**, 1085–1091 (2014).
42. Sullivan, D., Mizuseki, K., Sorgi, A. & Buzsáki, G. Comparison of sleep spindles and theta oscillations in the hippocampus. *J. Neurosci.* **34**, 662–674 (2014).
43. Wieser, H.G., Elger, C. & Stodieck, S. The 'foramen ovale electrode': a new recording method for the preoperative evaluation of patients suffering from mesio-basal temporal lobe epilepsy. *Electroencephalogr. Clin. Neurophysiol.* **61**, 314–322 (1985).
44. Ayoub, A., Mölle, M., Preissl, H. & Born, J. Grouping of MEG gamma oscillations by EEG sleep spindles. *Neuroimage* **59**, 1491–1500 (2012).
45. Buzsáki, G. Hippocampal sharp waves: their origin and significance. *Brain Res.* **398**, 242–252 (1986).
46. Skaggs, W.E. *et al.* EEG sharp waves and sparse ensemble unit activity in the macaque hippocampus. *J. Neurophysiol.* **98**, 898–910 (2007).
47. Buzsáki, G., Logothetis, N. & Singer, W. Scaling brain size, keeping timing: evolutionary preservation of brain rhythms. *Neuron* **80**, 751–764 (2013).
48. Ngo, H.-V.V., Martinetz, T., Born, J. & Mölle, M. Auditory closed-loop stimulation of the sleep slow oscillation enhances memory. *Neuron* **78**, 545–553 (2013).
49. Gais, S., Mölle, M., Helms, K. & Born, J. Learning-dependent increases in sleep spindle density. *J. Neurosci.* **22**, 6830–6834 (2002).
50. Girardeau, G., Benchenane, K., Wiener, S.I., Buzsáki, G. & Zugaro, M.B. Selective suppression of hippocampal ripples impairs spatial memory. *Nat. Neurosci.* **12**, 1222–1223 (2009).

ONLINE METHODS

Participants. The iEEG was recorded from patients suffering from pharmacoresistant epilepsy at the Department of Epileptology, University of Bonn. Depth electrodes were implanted stereotactically, either via the occipital lobe along the longitudinal axis of the hippocampus or laterally via the temporal lobe, during presurgical evaluation (the seizure onset zone could not be precisely determined with noninvasive methods). All patients received anticonvulsive medication (plasma levels within the therapeutic range). Each participant's drug regimen at the time of recordings is listed in **Supplementary Table 4** along with these drugs' documented effects on sleep (**Supplementary Table 5**). Informed consent for the iEEG recordings and the use of the data for research purposes was obtained from all patients. The study was approved by the ethics committee of the Medical Faculty of the University of Bonn.

Depth electroencephalograms were referenced to linked mastoids and recorded with a sampling rate of 1 kHz (bandpass filter: 0.01 Hz (6 dB per octave) to 300 Hz (12 dB per octave)). A total of 17 patients participated. Three participants were excluded because the seizure onset zone could not be unequivocally localized to one hemisphere, one participant was excluded because time spent in NREM sleep was below two z-scores of the group mean and one participant was excluded because the spindle detection algorithm yielded less than 100 spindle events (both providing insufficient data for the main analyses). Of the remaining 12 participants, six were female, mean age was 34 years (range 22–49) and the average duration of epilepsy was 20 years (range 10–43). Diagnostic evaluation revealed unilateral hippocampal sclerosis in six patients, unilateral extrahippocampal lesions in three patients and no clear lesions, but a unilateral EEG focus in three patients. 11 of the remaining patients were implanted with depth electrodes along the longitudinal axis of the hippocampus and one patient was implanted with depth electrodes laterally via the temporal lobe. To address the concern that hippocampal data might be contaminated by cortical signals picked up by the mastoid references (for example, global SOs), we also conducted the main analysis after re-referencing the hippocampal data to another contact on the same depth electrode. As shown in **Supplementary Figure 10**, the same pattern of results was observed, ruling out spurious referencing effects in our data.

Data processing, sleep stage classification and artifact rejection. For the sleep recordings, additional electrodes were placed on participants' scalps at positions Cz, C3, C4 and Oz according to the 10–20 system. Electroocular activity (EOG) was recorded at the outer canthi of both eyes and submental electromyographic activity (EMG) was acquired with electrodes attached to the chin. Interelectrode impedances were all below 5 k Ω .

The continuous raw data from Cz and the hippocampus were epoched into 20-s intervals for sleep staging and classified as wake, stage 1, stage 2, stage 3, stage 4 or REM sleep. Sleep stages were identified based on scalp electrodes together with concurrently monitored EOG and EMG according to standard criteria²². For subsequent analyses, stages 2, 3 and 4 were collapsed and denoted non-REM (NREM) sleep (equivalent to combining N2 and N3 according to ref. 51).

Given the central role of sleep spindles in the hypothesized oscillatory coupling (being modulated by SOs and in turn modulating ripples), the hippocampal contact with the largest peak in the spindle frequency range (12–16 Hz) was chosen based on the NREM/WAKE power spectrum ratios. As shown in **Supplementary Figure 1**, such relative sleep-related increase in spindle power tended to be the strongest in posterior hippocampal contacts. This was corroborated by a repeated-measures ANOVA with the factor Position (contact 1 to 10; including the 11 participants with the same longitudinal implantation scheme): $F(2,32,23.19) = 4.01$, $P = 0.027$, with a significant linear increase from anterior to posterior contacts ($F(1,10) = 9.68$, $P = 0.011$).

Analysis was performed with MATLAB (MathWorks), using the FieldTrip⁵² and CircStat⁵³ toolboxes as well as custom MATLAB functions. Preprocessing of the EEG data consisted of line noise removal (2-Hz bandstop filters centered at 50 Hz and its harmonics up to 200 Hz) and was followed by an automated artifact rejection algorithm: For each stage separately, each time point was converted into a z-score based on the participant- and stage-specific mean and s.d. of absolute amplitude, gradient (the amplitude difference between two adjacent time points) and amplitude of the data after applying a 250-Hz high pass filter (an additional means to identify epileptogenic spikes). A time point was then

marked as artifactual if it exceeded either a z-score of 5 in any of these measures or a conjunction of an amplitude z-score of 3 and a gradient- or high-frequency z-score of 3. The 1,000 ms preceding as well as the 1,000 ms following detected artifact samples were also marked as artifacts. We found that the combination of raw EEG amplitude, raw EEG gradient and EEG amplitude after highpass filtering the data at 250 Hz proved highly sensitive to detect epileptiform and other artifacts, as verified by manually identifying artifacts in random sub-selections of the data. To counter the potential concern that the automated artifact rejection procedure might be too conservative, we also conducted the analyses after raising the artifact detection thresholds. Here, a time point was marked as artifactual if it exceeded either a z-score of 6 (instead of 5) in amplitude/gradient/250-Hz high pass filtered amplitude or a conjunction of an amplitude z-score of 4 and a gradient- or high frequency z-score of 4 (both instead of 3). Results from this procedure are listed **Supplementary Table 3**, showing that the same pattern of PAC results emerged after raising the artifact detection thresholds.

Event-locked analysis. To assess PAC for specific, a priori defined oscillatory events of interest, that is, SO-to-spindle PAC (0.75 Hz to 12–16 Hz) and spindle-to-ripple PAC (12–16 Hz to 80–100 Hz), we conducted the following analyses separately for scalp EEG (Cz) and hippocampal iEEG (HC).

Event detection and extraction. SO, spindle and ripple events were identified independently for each participant and channel based on established detection algorithms^{15,23}. SOs were detected as follows. First, data were filtered between 0.16–1.25 Hz (two-pass FIR bandpass filter, order = 3 cycles of the low frequency cut-off), and only artifact-free data from NREM sleep stages 2–4 were used for event detection. Second, all zero-crossings were determined in the filtered signal, and event duration was determined for SO candidates (that is, down-states followed by up-states) as time between two successive positive-to-negative zero-crossings for Cz and two successive negative-to-positive zero-crossings for HC, respectively. Events that met the SO duration criteria (minimum of 0.8 and maximum of 2 s, 0.5–1.25 Hz) entered the next step. Third, event amplitudes were determined for the remaining SO candidates (trough-to-peak amplitude between two positive-to-negative zero crossing for Cz; peak-to-trough amplitude between two negative-to-positive zero-crossing for HC). Events that also met the SO amplitude criteria ($\geq 75\%$ percentile of SO candidate amplitudes, that is, the 25% of events with the largest amplitudes) were considered SOs. Manual validation in a random sampling of the raw EEG data yielded good agreement between hand-scored and algorithmically identified SOs, however with greater sensitivity of the automated algorithm for SOs that were less pronounced against the background EEG activity. Finally, artifact-free epochs (–2.5 to +2.5 s) time-locked to the SO down-state in the filtered signal were extracted from the unfiltered raw signal for all events.

Spindles were detected as follows. First, data were filtered between 12–16 Hz (two-pass FIR bandpass filter, order = 3 cycles of the low frequency cut-off), and only artifact-free data from NREM sleep stages 2–4 were used for event detection. Second, the r.m.s. signal was calculated for the filtered signal using a moving average of 200 ms, and the spindle amplitude criterion was defined as the 75% percentile of RMS values. Third, Whenever the signal exceeded this threshold for more than 0.5 s but less than 3 s (duration criteria) a spindle event was detected. Again, manual validation in a random sampling of the raw EEG data yielded good agreement between hand-scored and algorithmically identified spindles, however with greater sensitivity of the automated algorithm for spindles that were less pronounced against the background EEG activity. Finally, artifact-free epochs (–2.5 to +2.5 s) time-locked to the maximum spindle trough in the filtered signal were extracted from the unfiltered raw signal for all events.

Ripples were detected as follows. First, data were filtered between 80–100 Hz (two-pass FIR bandpass filter, order = 3 cycles of the low frequency cut-off), and only artifact-free data from NREM sleep stages 2–4 were used for event detection. Second, the r.m.s. signal was calculated for the filtered signal using a moving average of 20 ms, and the ripple amplitude criterion was defined as the 99% percentile of RMS values. Third, whenever the signal exceeded this threshold for a minimum of 38 ms (encompassing ~3 cycles at 80 Hz) a ripple event was detected. In addition, we required at least three discrete peaks or three discrete troughs to occur in the raw signal segment corresponding to the above-threshold RMS segment. This was accomplished by identifying local maxima or minima in the respective raw signal segments after applying a one-pass moving average filter

including the two adjacent data points. Fourth, artifact-free epochs (-1.5 to $+1.5$ s) time-locked to the maximum ripple peak in the filtered signal were extracted from the unfiltered raw signal for all events.

Time-frequency analysis. TFRs were calculated per event epoch (mtmconvol function of the FieldTrip toolbox) for frequencies from 5 Hz to 200 Hz in steps of 1 Hz using a sliding (SO: 10-ms steps; spindle and ripple: 5-ms steps) Hanning tapered window with a variable, frequency-dependent length that always comprised a full number of cycles (but at least five cycles and at least 100-ms window length, to ensure reliable power estimates for higher frequencies for which five cycles would result in too short windows). Time-locked TFRs of all epochs were then normalized as percent change from pre-event baseline (-2.5 to -1.5 s for SOs and spindles, -1.5 to -1.0 s for ripples) and averaged per participant.

Time-frequency statistics. For group level statistics, a two-tailed paired-samples t tests against the pre-event baseline interval was then used to test for a significant event-locked power changes (baseline-corrected values were normally distributed in SO-locked, spindle-locked and ripple-locked TFRs, Kolmogorov-Smirnov values < 0.18 , $P > 0.19$). To correct for multiple comparisons (SO-triggered: -2 s to $+2$ s \times 5–200 Hz; spindle-triggered: -2 s to $+2$ s \times 50–200 Hz; ripple-triggered: -1 s to $+1$ s \times 5–30 Hz), a cluster-based permutation procedure was applied as implemented in FieldTrip⁵⁴. The initial threshold for cluster definition was set to $P < 0.01$ and the final threshold for significance of the summed t value within clusters was set to $P < 0.05$.

Preferred PAC phases. For all time points in each extracted event epoch, the phase values of the lower-frequency (modulating) oscillatory event as well as the phase values of the power fluctuation of the higher-frequency (modulated) oscillation (that is, TFR bins averaged across the respective frequencies and up-sampled from the respective time resolution of the TFR to the sampling frequency of 1,000 Hz) were extracted using the Hilbert transform. To ensure proper phase estimation, both lower- and faster-frequency time series were filtered beforehand in the range of the modulating event of interest (SO: 0.5–1.25 Hz; spindle: 12–16 Hz; two-pass FIR bandpass filter, order = 3 cycles of the low frequency cut-off). As suggested previously⁵⁵, the synchronization index (SI) was then calculated between the two phase value time series for each event epoch. The resulting SI is a complex number of which the angle represents the ‘preferred phase’ of the synchronization (SI_p), that is, the phase of the lower frequency at which the power of the higher frequency is maximal across time

$$SI = \frac{1}{n} \times \sum_{t=1}^n e^{i \times [\varphi_{it} - \varphi_{ut}]}$$

where n is the number of time points, φ_{it} is the phase value of the fluctuations in the upper frequency power time series at time point t , and φ_{ut} is the phase value of the lower frequency band time series at time point t ⁵⁶. The interval for estimating the preferred phase was -1 s to $+1$ s around the SO center and -0.25 s to $+0.25$ s around the spindle center.

Preferred PAC phase statistics. In case of a priori specified directions of phase angles, a powerful alternative to the Rayleigh test is the V test, which tests for non-uniformity of circular data with a specified mean direction⁵³. In particular, the alternative hypothesis H_1 states that the population is clustered around a known mean direction, whereas the H_0 states that the population is either unclustered (that is, uniformly distributed around the circle) or is clustered elsewhere, that is, different from the pre-specified direction. In the current case there were clear predictions with regard to the expected modulations, that is, SO-spindle modulation at the SO up-state (0° in Cz recordings, 180° in HC recordings)^{4,5,15} and spindle-ripple modulation at the spindle trough (180°)^{4,5}.

Peri-event time histograms. To visualize the temporal relationship of different event types (SOs, spindles and ripples) with respect to each other, we plotted PETHs in which the temporal occurrence of a ‘target’ event type is depicted with respect to a ‘seed’ event type (for example, **Supplementary Fig. 6a** plots the temporal occurrence of SOs (target) with respect to spindles (seed, time 0)). Histograms were created for each participant individually using MATLAB’s ‘histc’ function (100-ms bins from -5 s to $+5$ s or, for the ripple-ripple PETH in **Fig. 4c**, 10-ms bins

from -0.5 s to $+5$ s) and then averaged across participants. Bars are always normalized to sum up to 100% across the display interval.

Comodulogram analysis. To assess PAC simultaneously for a large number of frequency pairs, we applied a previously described method³⁵. Briefly, for a given frequency pair, the raw EEG signal was filtered separately in both frequencies (two-pass finite-impulse-response (FIR) bandpass filter, order = 3 cycles of the low frequency cut-off). Lower frequencies ranged from 0.75–20 Hz (0.5-Hz increments, 1-Hz filter bandwidth) and higher frequencies from 3–200 Hz (1-Hz increments with 2-Hz filter bandwidth from 3–29 Hz and 5-Hz increments with 10-Hz filter bandwidth from 30–200 Hz). The time series of the lower frequency phase and the higher frequency amplitude were then extracted using the Hilbert transform. The lower-frequency phases were binned into 18 20° bins ($n_{bins} = 18$) and for each bin the mean amplitude of the higher-frequency was computed and then normalized by dividing it by the sum over all bins. Next, the MI was computed, which assesses whether there is a measurable deviation of the amplitude distribution P from a uniform distribution U .

$$MI = \frac{D_{KL}(P,U)}{\log(n_{bins})}$$

The Kullback–Leibler (KL) distance, $D_{KL}(P,U) = \log(n_{bins}) - H(P)$, where the Shannon entropy H of the distribution P , $H(P) = -\sum_{ibin=1}^N P(ibin) \times \log[P(ibin)]$.

If $P = U$, that is, the higher-frequency amplitude is the same for each bin of the lower-frequency phase, $MI = 0$. Conversely, a MI equal to 1 would be observed if P had a Dirac-like distribution ($P = 1$ for a given bin and 0 for all the other bins).

For the comodulogram analysis, epochs were defined as 12 s of continuous artifact-free EEG data, surrounded by additional 2 s of artifact-free data for filter padding. The epoch length of 12 s was dictated by the lowest frequency of interest (0.25 Hz, that is, a 1-Hz bandwidth filter centered on 0.75 Hz) in combination with a filter order set to three cycles of the low frequency cut-off. Prior to entering the comodulogram analysis, the resulting 14-s epochs were subjected to additional visual artifact inspection using FieldTrip’s `ft_rejectvisual` function on the raw data and again after highpass filtering the data at 250 Hz, using its `absmax` and `var` summary functions. To accommodate different epoch numbers across participants and stages after artifact rejection [NREM: 346 (s.d. = 184), WAKE: 246 (s.d. = 212)], we calculated, separately for each stage, one MI for 50 concatenated epochs (equivalent to 10 min of recordings), ensuring that the dependent measure was always based on the same amount of data. This was repeated for all available iterations of 50 epochs and the resulting MI s were then collapsed within a given stage and carried forward to second-level statistics across participants. Note that because the MI is based on continuous sleep recordings rather than on discrete oscillatory events, this measure may still be driven by discrete occurrences of transient SO and spindle events, but is also sensitive to more sustained or stationary PAC. Surrogate PAC data were derived by calculating the MI where the modulating frequency came from epoch n and the modulated frequency came from epoch $n+1$. Note that by using two adjacent epochs (barring artifact-rejected data) rather than a random combination of phase- and amplitude providing epochs, this procedure is particularly conservative by also accounting for potential slow signal fluctuations across temporally proximal epochs. Across both comparisons (NREM versus NREM_surrogates, NREM versus WAKE), the MI values were normally distributed (Kolmogorov-Smirnov value = 0, $P = 0.189$).

Statistics summary. Statistical analyses were performed with MATLAB (MathWorks), using the FieldTrip⁵² and CircStat⁵³ toolboxes as well as custom MATLAB functions. Both parametric tests (t test, ANOVA) and non-parametric tests (permutation tests) were used. $P < 0.05$ was considered significant unless stated otherwise.

Event-locked analyses. For time-frequency statistics comparing percent power changes from baseline at the group level, we used a priori two-tailed paired-samples t tests and two-way repeated measures ANOVAs followed by *post hoc* paired t tests were applicable. Data were normally distributed as indicated by non-significant Kolmogorov-Smirnov tests. Correction for multiple comparisons

was applied using the cluster-based permutation procedure implemented in FieldTrip⁵⁴. For preferred PAC phase statistics at the group level, the *V*-test was used to test for non-uniformity of circular data with a specified mean direction⁵³. At the single-subject level the Rayleigh-test was used to test for non-uniformity of circular data with unspecified mean direction⁵³.

Comodulogram analyses. PAC, indicated by the MI, during NREM sleep was compared against both PAC during WAKE and NREM surrogate data using two-tailed paired *t* tests, and differences in the distribution of amplitude modulation across phase bins was compared between PAC clusters using a two-way repeated measures ANOVA. Data were normally distributed as indicated by non-significant Kolmogorov-Smirnov test. No statistical methods were used to pre-determine sample size, but our sample size ($N = 12$) was similar to that reported in related previous publications ($N = 11$ in ref. 17; $N = 9$ in ref. 18; $N = 7$ in ref. 19; $N = 13$ in ref. 9). Randomization was not applicable, as independent variables (for example, phase angles of ongoing neuronal oscillations) varied within-subject. Blinding was not applicable since neither participants nor

experimenter had any influence on the spontaneous oscillatory dynamics recorded during deep sleep, which were analyzed by fully automated scripts.

A **Supplementary Methods Checklist** is available.

51. Iber, C., Ancoli-Israel, S., Chesson, A. & Quan, S.F. *The AASM Manual for the Scoring of Sleep and Associated Events: Rules, Terminology and Technical Specifications* (American Academy of Sleep Medicine, 2007).
52. Oostenveld, R., Fries, P., Maris, E. & Schoffelen, J.-M. FieldTrip: open source software for advanced analysis of MEG, EEG, and invasive electrophysiological data. *Comput. Intell. Neurosci.* **2011**, 156869 (2011).
53. Berens, P. CircStat: a Matlab Toolbox for Circular Statistics. *J. Stat. Softw.* **31**, 1–21 (2009).
54. Maris, E. & Oostenveld, R. Nonparametric statistical testing of EEG-and MEG-data. *J. Neurosci. Methods* **164**, 177–190 (2007).
55. Mormann, F. *et al.* Phase/amplitude reset and theta-gamma interaction in the human medial temporal lobe during a continuous word recognition memory task. *Hippocampus* **15**, 890–900 (2005).
56. Cohen, M.X. Assessing transient cross-frequency coupling in EEG data. *J. Neurosci. Methods* **168**, 494–499 (2008).